Infrared radiometry-based background-compensated thermometric instrument for noncontact temperature and friction measurements

L. Li, A. Mandelis,[a] J. Garcia, and C. Eccles
Department of Mechanical and Industrial Engineering, Photothermal and Optoelectronic Diagnostics Laboratories, University of Toronto, Toronto M5S 3G8, Canada

(Received 11 December 2000; accepted for publication 18 February 2001)

The design and performance of a novel thermometric instrument featuring thermal-emission-intensity harmonic modulation, noncontact infrared radiometric detection, and stray background suppression is described. The instrumental principle depends on thermal (blackbody) emission of Planck radiation from a heated surface. It was developed to measure small temperature rises caused by frictional heating. A low-power He–Ne heating laser was used to investigate the sensitivity and estimate a figure-of-merit (FOM) for the instrument. Background compensation leading to signal baseline suppression was partly achieved with a differential mechanical chopper blade, designed to induce destructive interference of infrared radiation superposition from heated and reference spots on a ceramic sample coated with a metallic thin film. Additional background suppression was achieved by lock-in amplifier signal amplitude and phase compensation through an externally superposed wave at the same chopping frequency. The FOM of the noncontact thermometric instrument was 159.9 ± 8.5. The system sensitivity (minimum temperature rise) for the particular thin-film/ceramic material was estimated to be 0.18–0.23 °C. © *2001 American Institute of Physics.* [DOI: 10.1063/1.1364670]

I. INTRODUCTION

In space applications, it is known that the success or failure of robotic manipulators in replacing and installing objects transported from Earth to space vehicles, such as the Space Shuttle or the orbiting International Space Station will be determined in large part by the dynamic (sliding) friction coefficient between the various sliding surfaces. These friction coefficients cannot be determined by analysis and are not available in the literatures. Some sets of friction coefficients have been reported under Earth surface conditions.[1–4] Space-relevant friction coefficients, however, must be obtained under vacuum environment. The present work was motivated precisely by the need for measuring friction coefficients with high sensitivity in a noncontact manner from the thermal energy generated through friction, under vacuum where the only form of thermal energy transport is radiation heat transfer (thermal emission).

It has long been recognized that tribological measurements are notoriously unreliable as generalized friction performance indicators between specific surfaces. This occurs due to the very wide variability between measurements of nominally the same material interfaces.[5] Therefore, it is important to obtain actual friction coefficient measurements for all practical tribological interfaces of interest. Since friction can cause a temperature rise at the contact points, a radiation heat transfer field arises, which may be measured under ambient pressure or under vacuum conditions, according to Stefan's law:

$$S_{\text{blackbody}} = \epsilon \sigma T^4, \tag{1}$$

where $S_{\text{blackbody}}$ is the total radiant emissive power of a blackbody in thermal equilibrium, ϵ is the emissivity of the medium, T is the absolute temperature, and σ is the Stefan–Boltzmann constant, $\sigma = 5.6703 \times 10^{-8}\ \text{W/m}^2\,\text{K}^4$. For small temperature increases ΔT a linearized form of Eq. (1) is used[6]

$$\Delta S_{\text{blackbody}}(t) = 4 \epsilon \sigma T_0^3 \Delta T(z=0,t), \tag{2}$$

where T_0 is the ambient temperature. The conductive measurement of this temperature rise with satisfactory precision is very difficult by means of thermocouples. This article introduces a differential contact-free thermometric system, which can measure net temperature rise by detecting thermal infrared emission radiation from a continuous-laser-heated surface simulating a tribological interface.

II. DIFFERENTIAL INFRARED (IR) RADIATION AND TEMPERATURE MEASUREMENT INSTRUMENTATION

Figure 1 shows the overall experimental setup for the differential infrared radiation thermometric instrument. In this system, two ellipsoidal-arc mirrors were focused on two spatially separate spots on a sample surface, and were used to collect the blackbody radiation signal emitted from each spot within the solid angle subtended by the area of the inside surface of the appropriate mirror. The other foci of both ellipsoids were carefully adjusted to fully overlap on the active element of a HgCdTe [mercury–cadmium–telluride (MCT)] wide-bandwidth IR detector. The mirrors were machined from solid aluminum, and there was no reflective coating on their inner (concave) surfaces. Their reflectivity

[a]Author to whom correspondence should be addressed: electronic mail: mandelis@mie.utoronto.ca

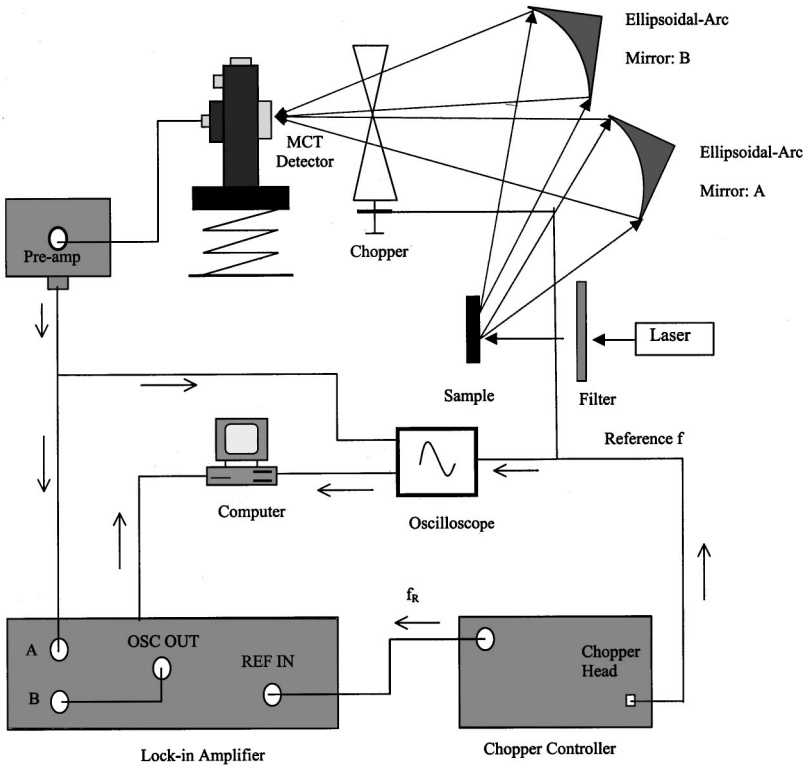

FIG. 1. Experimental setup of the differential compensated infrared radiometric thermometer.

was that of polished aluminum. Both mirrors had three translational and three rotational degrees of freedom for adjustment purposes, as shown in Fig. 2: They were held by adapter plates to a kinematic mount or gimbal, which provided two degrees of freedom of rotation: θ_1 and θ_2. Each gimbal was positioned with three translational stages configured such that each one was aligned with either the *x*, *y*, or *z* axis. The stages were in turn mounted on a goniometer. This device allowed a third degree of freedom for rotation θ_3. Furthermore, there were three screw adjustments at the back of each mirror on the gimbals so that the mirrors could be further adjusted finely. The lower of the two ellipsoidal-arc mirrors transmitted infrared radiation from an optically heated spot on a flat sample surface, while the upper one was focused at a reference spot on the same surface, approximately 5 mm away from the heated area. This distance was assumed to be adequate for conduction heat transfer from the heated area to be negligible and thus not perturb the temperature of the reference spot.

A specially designed differential mechanical chopper blade allowed radiation from one spot to enter the IR detector during 50% of the selected intensity-modulation period through an opening (slot) subtending an arc of 180°. During the remaining 50% of each period, radiation from the other spot entered the detector through a second slot, which also subtended an arc of 180°. The shape of the differential chopper blade with two slots is shown in Fig. 3(a), along with the shapes of two single-slot blades used for monitoring radiation leakage (''crosstalk''), Figs. 3(b) and 3(c) (see Sec. III). The output of the IR detector was preamplified and fed into a lock-in amplifier (LIA) for demodulation. The output signal was stored in a PC. The time-repetitive wave form could also be displayed in a transient oscilloscope (HP 54200D). Several transients could be coadded in the oscilloscope, and the data could be transferred to, stored in, and displayed on a computer screen by means of appropriate software. When the temperature of both sample surface spots is the same, assum-

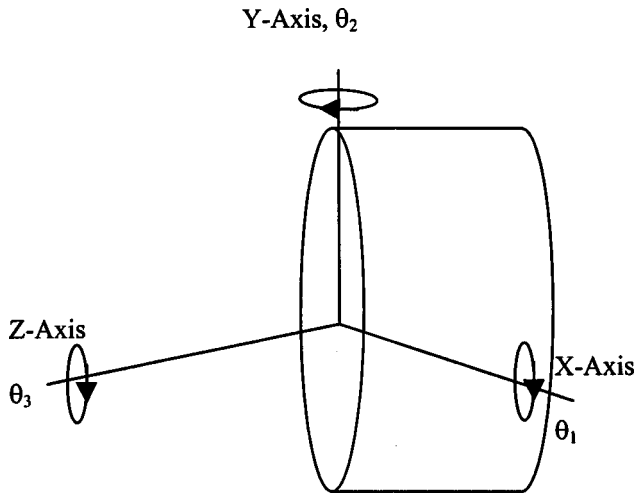

FIG. 2. Schematic of ellipsoidal-arc mirror translational and rotational degrees of freedom.

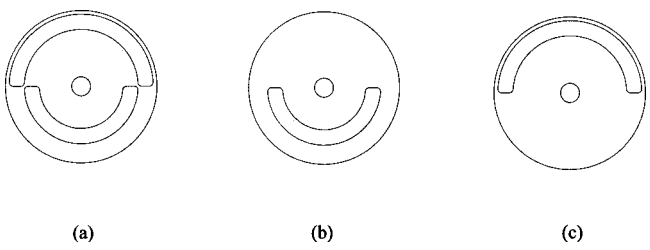

FIG. 3. Three chopper-blade designs: double-slot blade for differential IR signal generation (a); and single-slot blades for optical crosstalk tests and instrumental figure-of-merit calculations (b), (c).

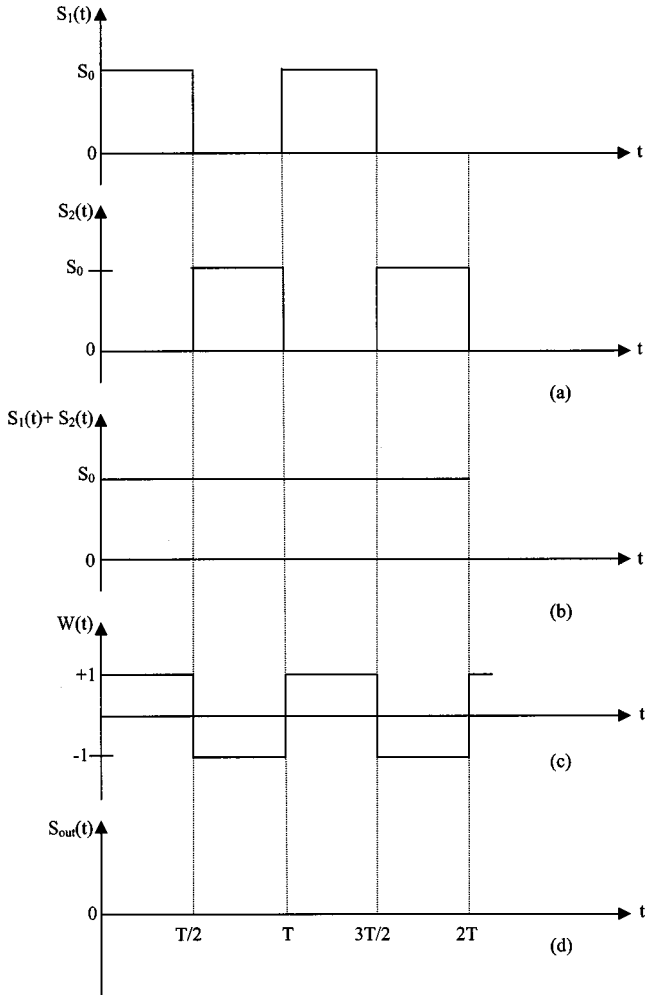

FIG. 4. Lock-in wave form sequences due to the temporal superposition of two signals $S_1(t)+S_2(t)$ generated by chopping two IR thermal radiation emission bundles with the double-slit chopper of Fig. 3(a). $W(t)$: lock-in weighting wave form. S_{out}: time-independent demodulated lock-in signal output. The scheme is only valid for long LIA time constants compared to waveform repetition period T (see Ref. 7).

ing identical materials with identical surface emissivities and collection optics, the signal output from the instrumental design of Fig. 1 is expected to be ideally zero. This occurs because the demodulated LIA output signal is the integral (area) of the input wave form during the first half cycle minus the integral (area) of the input wave form during the second half cycle.[7] For identical half wave forms and zero instrumental phase delay (alignment of the LIA reference square wave rising edge with the onset of the external incident wave form), this signal generation scheme implies that equal areas are swept along the time axis. Therefore, the result of the signal demodulation (integral/area subtraction between $[0,T/2]$ and $[T/2,T]$ segments) is zero for all types of wave forms. This signal generation principle is illustrated in Fig. 4 and it is the temporal analog of destructive interference due to spatial superposition of two out-of-phase waves. Here, for simplicity, two superposed square wave forms of equal intensities S_0 are assumed entering the LIA over one modulation period T.

The heated surface consisted of a thin metallic strip coating, 0.3 μm thick, made of a Au–Cr alloy, coated on a ceramic substrate (''sitall''). This ceramic is a high-conductivity material based on SiO_2–Al_2O_3 and is used as a heat sink in the Russian microelectronics industry.[8] The sitall thickness was ~1 mm. The emitted IR radiation signals from the surface of the sample were chopped and detected by the MCT detector. When the chopper was used to modulate the dc signal of interest, however, the background radiation was also chopped synchronously. These background signals could affect the value of the output LIA signal significantly and compromise the sensitivity of the thermometric instrument by means of the large signal baseline. As expected, it was found that the differential signal, generated by the superposition of the two infrared wave forms modulated out-of-phase, effectively minimized the background signal. This minimization was found to be a figure-of-merit (FOM) for the radiometric temperature-measuring instrument. After the two ellipsoidal-arc mirrors and the MCT detector were properly positioned, the chopper blade position was optimized for maximum radiation collection. In order to minimize the interference of chopped background radiation signals, a large direct current was allowed to flow in the metallic Au–Cr coating acting as a strip heater through the application of an external dc bias across the coating. In this manner the background radiation signal became much smaller than those from the Joule-heated surface, allowing the position of the chopper blade to be adjusted for maximum LIA output signal.

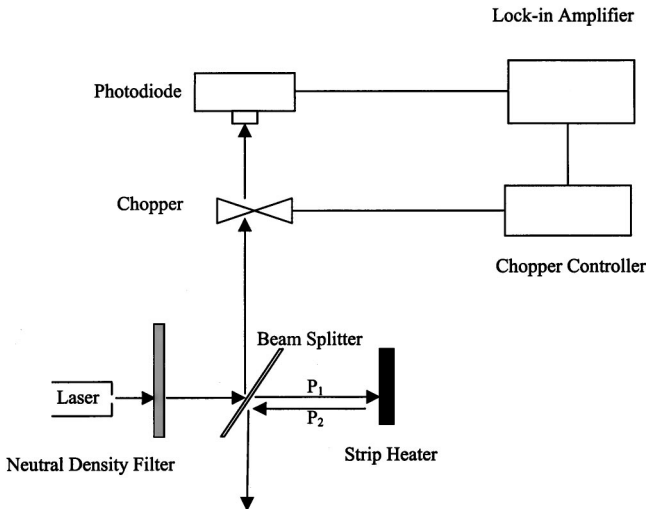

FIG. 5. Schematic of the laser beam power calibration.

III. EXPERIMENTAL AND RESULTS

A 2 mW He–Ne laser was used to generate optical heating on the sample surface at the focal spot of the lower ellipsoidal-arc mirror. The laser beam was a Gaussian of ~2 mm diameter. Several combinations of neutral density filters were placed between the laser beam and the metal coating of the sample surface to produce various incident intensities. To measure the power of the laser beam incident on the metal strip, a microscope slip beamsplitter was used as shown in Fig. 5. The small fraction (14.74%) of the laser beam thus separated was chopped and directed to a photodiode, the output of which was fed into a LIA. This optical setup allowed

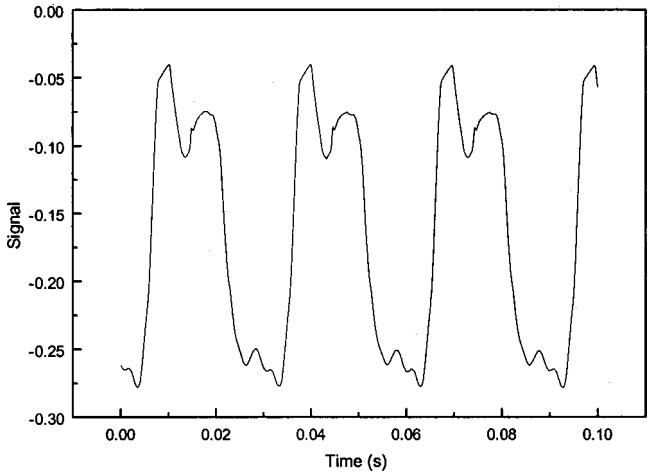

FIG. 6. Co-added transient MCT wave form generated with the chopper blade of Fig. 3(b).

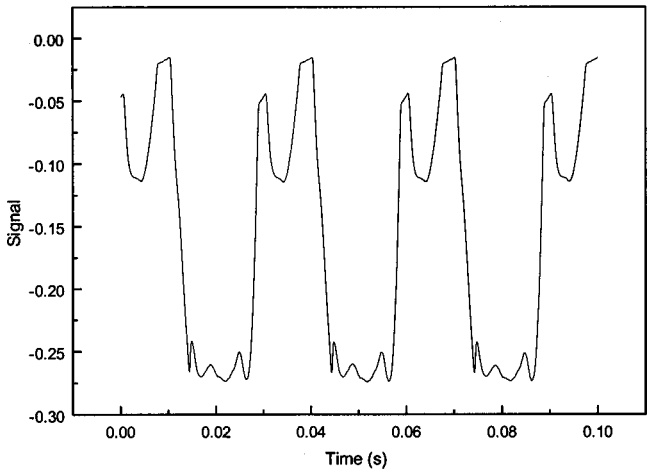

FIG. 7. Co-added transient MCT wave form generated with the chopper blade of Fig. 3(c).

accurate measurements of a wide range of low, sub-mW, laser powers, which were not possible with commercial laser power meters. The fraction A of incident laser power directed to the sample was

$$A=\frac{P_{10}-P_{20}}{P_{10}}=\frac{P_{1F}-P_{2F}}{P_{1F}}=\text{const}, \tag{3}$$

where $P_{10}(P_{20})$ is the incident (reflected) laser power on the sample without neutral density filters reducing the beam intensity; and $P_{IF}(P_{2F})$ are the same definitions of power past a neutral density filter, which allows only a fraction F of the incident radiation to be transmitted. P_{10} and P_{20} were also measured using the setup of Fig. 5. The actual laser-beam power P absorbed by the metallic strip sample can be calculated by

$$P=P_{10}\left(\frac{S_F}{S_0}\right)A, \tag{4}$$

where, S_F is the LIA readout due to the split-off laser beam with the neutral density filter in place, and S_0 denotes the same LIA signal readout without the neutral density filter.

In order to test radiation leakage and the efficiency of destructive interference on the MCT, the three chopper blades of Fig. 3 were used without laser heating. Each of the single-opening blades of Figs. 3(b) and 3(c) had its slot located at a different distance from the rim, designed to receive radiation mainly from only one (upper or lower) of the two ellipsoidal-arc mirrors. Each blade was further positioned so as to maximize the IR radiation throughput from the corresponding mirror. Figures 6 and 7 show coadded traces of the repetitive IR wave forms produced from these two chopper blades at room temperature without laser heating, as they were captured by the transient scope. When the chopper blade [Fig. 3(b)] was used and the radiation from the surface spot, which was mainly collected by the ''other'' mirror corresponding to the chopper blade [Fig. 3(c)] was blocked, this operation had minimal or no effect on the wave forms shown in Figs. 6 and 7. The reverse was also true. Therefore, it was concluded that there was negligible radiation leakage from each mirror through the chopper-blade slot associated with the other mirror. The chopper blade with the double opening, [Fig. 3(a)] had the slots cut at exactly the same locations as each one of the single-slot chopper blades, thus ensuring that optical ''crosstalk'' (leakage) would be negligible. The resulting superposition wave form from the two spots at ambient temperature is shown in real time in Fig. 8. It should be noted that the average peak-to-baseline signal intensity in the repetitive wave form of Fig. 8 is ~0.06 arbitrary units (a.u.), whereas that of both wave forms in Figs. 6 and 7 is ~0.26 a.u. This indicates that the signal superposition yields a destructive interference pattern, which suppresses the resultant modulated signal by a factor of ~4.5.

The foregoing tests were repeated with laser heating of the surface spot associated with the upper mirror and the chopper blade with the inside opening of Fig. 3(b). The LIA signal was recorded for a number of incident laser powers produced by a series of neutral density filters. Figure 9 shows the LIA amplitude as a function of incident laser power. The corresponding results with the two-slot chopper blade [Fig. 3(a)] are shown in Fig. 10. It can be seen from Figs. 9 and 10 that the chopper blade [Fig. 3(a)] acts as a differential common-mode rejection element, suppressing large part of

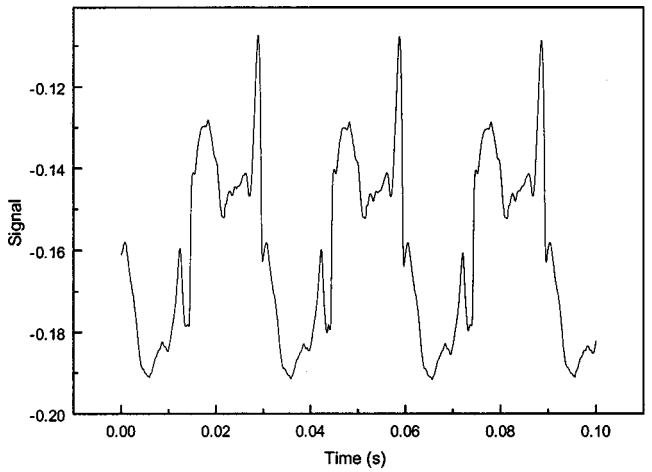

FIG. 8. Coadded transient MCT wave form generated with the two-slot chopper blade of Fig. 3(a).

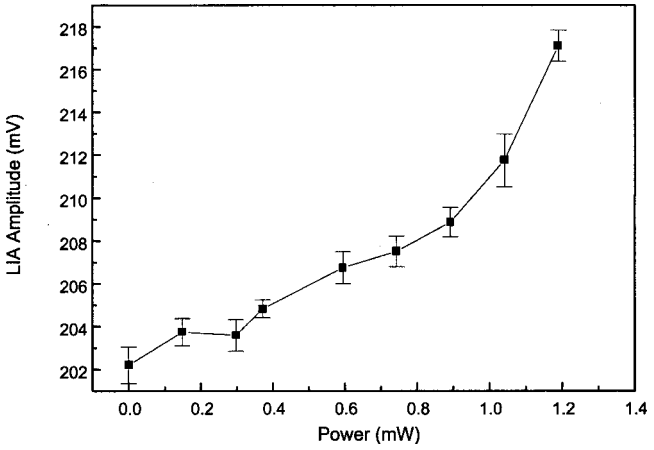

FIG. 9. LIA amplitude vs laser power curve with the chopper blade of Fig. 3(b).

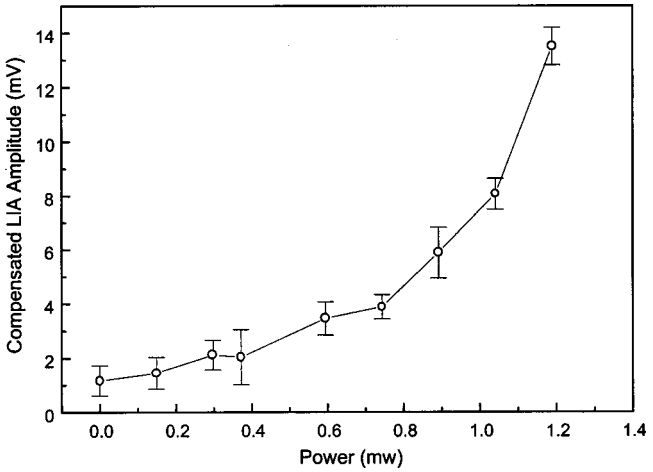

FIG. 11. LIA amplitude vs laser power curve with the chopper blade of Fig. 3(b) and external LIA-wave form amplitude and phase compensation.

the IR background common to both radiation-emitting surface spots. Repeating the experiments of Figs. 9 and 10 with the other single-slot chopper blade [Fig. 3(c)] corresponding to the nonheated (reference) spot, no LIA signal change from the background value with changes in incident laser power was observed. These results are consistent with the negligible crosstalk findings during the tests of Figs. 6–8 using the transient scope.

Using the average lock-in amplifier signals from the three chopper blades under no external heating, several FOM can be calculated for the thermometric instrument. The most important FOM is the one associated with the laser-heated spot, and is calculated from

$$\mathrm{FOM}_I = \frac{S_I}{S_B}. \tag{5}$$

Another FOM is associated with the reference spot

$$\mathrm{FOM}_O = \frac{S_O}{S_B}. \tag{6}$$

Here, S_I, S_O, and S_B are the LIA amplitudes with chopper blade [Fig. 3(b)] (inside slot), with chopper blade [Fig. 3(c)] (outside slot) and with chopper blade [Fig. 3(a)] (two slots), respectively. The experimental results gave $\mathrm{FOM}_I = 4.05 \pm 0.14$ and $\mathrm{FOM}_O = 4.07 \pm 0.15$. These demodulated LIA signal FOMs are in agreement with the transient wave form magnitudes of Figs. 6–8.

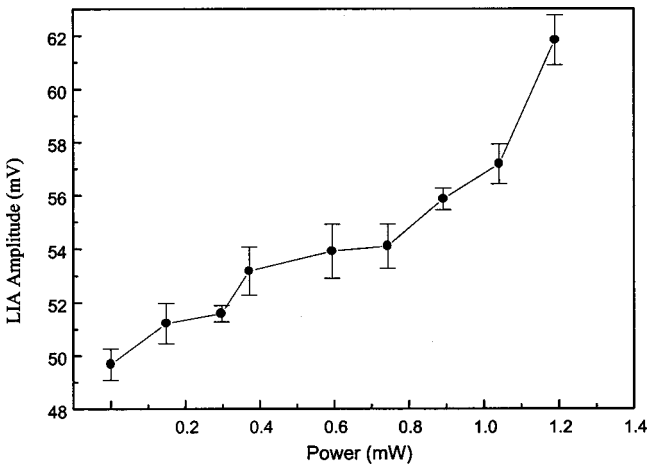

FIG. 10. LIA amplitude vs laser power curve with the two-slot chopper blade of Fig. 3(a).

Figure 10 shows that the signal due to ambient IR background can be suppressed, but not fully eliminated with the two-slot blade. An instrumental LIA compensation scheme particular to the EG&G DSP LIA Model 7265 was thus implemented to further minimize the stray background signal from the data.[9] As shown in Fig. 1, the internal oscillator of the LIA (OSC OUT) was turned on with the same frequency as that of the chopper, and the OSC OUT signal was fed into channel B. Its amplitude was then adjusted to be equal to the value of the unsuppressed IR background in channel A. With the auto phase function of the LIA channels A and B had the same phase. By selecting the signal output setting (channel A) to the operation (A–B), the ambient IR background was thus fully eliminated. Figure 11 shows the LIA amplitude versus laser intensity using the two-slot blade with this compensation scheme. From the laser-off point (0 mW) it can be seen that the background signal is completely eliminated within the experimental error. The FOM of the fully background-compensated system is given by the ratio of the LIA amplitude using the single-slot chopper blade to that using the two-slot blade plus external compensation, at constant incident laser power. This was estimated (at the laser off point, 0 mW) from the data of Figs. 9 and 11 to be

$$\mathrm{FOM}_{\max} \approx 159.9 \pm 8.5.$$

IV. THEORETICAL SIGNAL ANALYSIS AND INSTRUMENTAL SENSITIVITY

In order to calculate the approximate temperature rise that the IR thermometric instrument can sense, a photothermal model of the temperature field due to a Gaussian laser beam was developed as shown in Fig. 12. A continuous Gaussian laser beam impinges on a ceramic sample with a 0.3 μm thick metallic surface coating. Therefore, the thermal mass of the coating was considered to be negligible, and the effect of the coating itself on the temperature was confined to

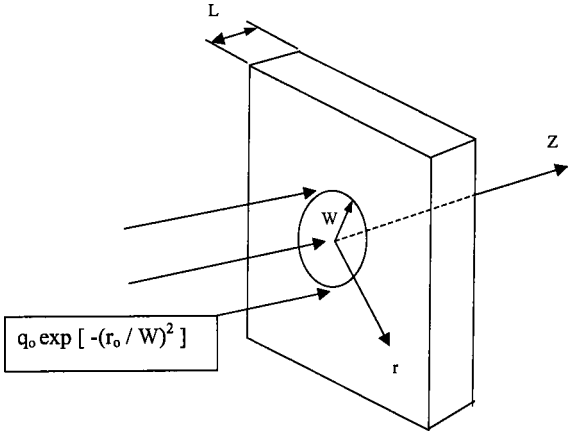

FIG. 12. Schematic of the mathematical model for the cylindrically symmetric temperature field due to a heating Gaussian laser beam of spotsize W, incident on a thermally isotropic solid of thickness L.

its reflectivity R. The temperature rise can be calculated by means of the Green function method in cylindrical coordinates due to the symmetry imposed by the Gaussian laser beam source. The cylindrical thermal Green function in an isotropic layer of thickness L, $0 \leqslant z \leqslant L$, and infinite lateral dimensions, with thermal flux prescribed on the surface $0 \leqslant r$ is easily obtained from the thermal-wave Green function representation as an inverse Hankel transform[10] in the limit of zero modulation frequency:

$$G(r,z|r_0,z_0)=\frac{1}{4\pi\alpha}\int_0^\infty \frac{J_0(\lambda r)J_0(\lambda r_0)d\lambda}{1-e^{-2\lambda L}} \times[e^{-\lambda|z-z_0|}+e^{-\lambda(z+z_0)}+e^{-\lambda(2L-|z-z_0|)} +e^{-\lambda(2L-(z+z_0))}], \tag{7}$$

where $J_0(x)$ is the Bessel function of the first kind of order zero, and λ is the Hankel space variable. α is the substrate thermal diffusivity. The Green function Eq. (7) satisfies homogeneous Neumann boundary conditions at the surfaces $z=0$, L. Assuming a Gaussian distribution of the surface temperature through absorption of the incident laser beam power, the Hankel transform of the temperature $T(r,z)$ at any depth z becomes[10]

$$\tau_H(\lambda,z)=(1-R)\frac{\pi\alpha q_0}{k} \times\int_0^\infty e^{-(r_0/w)^2} g(\lambda,z|r_0,0)r_0\,dr_0. \tag{8}$$

Here q_0 is the thermal flux at the surface (W/m^2) and k is the material thermal conductivity (W/mK). W is the laser beam spot size and R is the surface reflectance. $g(\lambda,z|r_0,z_0)$ is the Hankel transform of the Green function, Eq. (7). For the purpose of calculating the front-surface temperature of the ceramic substrate sitall, we may let the thickness of the solid in Fig. 12 ($\sim$1 mm) become infinite, a very good approximation for wave form repetition periods on the order of 100 Hz, in which case the infinite inter-reflections of thermal energy which comprise the denominator of Eq. (7) are eliminated. Letting $L\to\infty$, we find[10]

$$g(\lambda,z|r_0,z_0)=\frac{J_0(\lambda r_0)}{4\pi\alpha\lambda}[e^{-\lambda|z-z_0|}+e^{-\lambda(z+z_0)}]. \tag{9}$$

Therefore, taking the inverse Hankel transform of Eq. (8)

$$T(r,z)=(1-R)\frac{q_0W^2}{k}\int_0^\infty e^{-\lambda z-(\lambda^2W^2/4)}J_0(\lambda r)d\lambda. \tag{10}$$

On the surface

$$T(r,0)=(1-R)\frac{q_0W^2}{k}\int_0^\infty e^{-(\lambda^2W^2/4)}J_0(\lambda r)d\lambda. \tag{11}$$

Using the formula

$$\int_0^\infty e^{-ax^2}J_v(\beta x)dx=\frac{\sqrt{\pi}}{2\sqrt{\alpha}}e^{-(\beta^2/8\alpha)}I_{\nu/2}\left(\frac{\beta^2}{8\alpha}\right) \tag{12}$$

in Ref. 11, entry 6.618, p. 710, we obtain an analytical expression for the integral Eq. (11):

$$T(r,0)=(1-R)\frac{\sqrt{\pi}q_0W}{k}e^{-(r^2/2W^2)}I_0\left(\frac{r^2}{2W^2}\right), \tag{13}$$

where $I_v(x)$ is the Bessel function of the second kind of order v. Equation (13) allows the calculation of the *peak* surface temperature:

$$T(0,0)=(1-R)\frac{\sqrt{\pi}q_0W}{k}. \tag{14}$$

To estimate the *mean* temperature of the laser-heated surface, the integral of Eq. (13) over the area πW^2 defined by the beam spot size can be taken as

$$\overline{T}=(1-R)\frac{2\sqrt{\pi}q_0}{kW}\int_0^W e^{-(r^2/2W^2)}I_0\left(\frac{r^2}{2W^2}\right)r\,dr. \tag{15}$$

Using Ref. 11, entry 6.625.1, p. 713, we find

$$\overline{T}=(1-R)\frac{\sqrt{\pi}q_0W}{k}{}_1F_1\left(\frac{1}{2};2;-2\right), \tag{16}$$

where ${}_1F_1(a;b;x)$ is the degenerate hypergeometric function. This function has the series expansion (Ref. 11; entry 9.210.1, p. 1058)

$${}_1F_1(a;b;x)=1+\frac{a}{b}\frac{x}{1!}+\frac{a(a+1)}{b(b+1)}\frac{x^2}{2!} +\frac{a(a+1)(a+2)}{b(b+1)(b+2)}\frac{x^3}{3!}+\ldots. \tag{17}$$

Carrying out the calculation results in the mean surface temperature

$$\overline{T}\approx 0.65(1-R)\frac{\sqrt{\pi}q_0W}{k}. \tag{18}$$

The laser beam spot size W was measured to be 2 mm. The thermal conductivity of the substrate ceramic material ''sitall'' is 1.5 W/mk.[8] The incident thermal flux q_0 was obtained from the absorbed laser beam power P_1

$$q_0=\frac{P_1}{\pi W^2}, \tag{19}$$

with $R = P_2 / P_1 = 0.05$.

From the background baseline-compensated Fig. 11, we conclude that the laser beam power required to achieve the minimum measurable temperature rise that the system can sense is ~0.4–0.5 mW within 1 standard deviation. For this laser beam power, the mean temperature rise on the surface measured by the MCT detector is calculated from Eq. (18) to be

$$\overline{T}_{\min} \approx 0.18 - 0.23\ \mathrm{K}.$$

It is interesting to note that the sensitivity of our differential IR radiometric thermometer can improve proportionally to the solid angle subtended by (or to the collection area of) the ellipsoidal-arc mirror. The minimum temperature-detection limit of the present instrument compares very favorably with an uncompensated IR thermometer, with chopper intensity-modulated input and LIA-demodulated signal output, reported by Markham and Kinsella[12] for temperature measurements of turbine engines. Although no sensitivity limits are given by those authors, a noise floor of more than 1 °C centered about 700–1200 °C, with minimum detection temperature rise of 2–3 °C can be gleaned from their data curves.

ACKNOWLEDGMENTS

The authors gratefully acknowledge the support of the Natural Sciences and Engineering Council of Canada (NSERC), of the Canadian Space Agency (CSA), and of McDonald Detwiller (MD) Robotics for a grant that made this research possible.

[1] *Friction, Lubrication and Wear Technology, Appendix: Static and Kinetic Friction Coefficients for Selected Materials*, ASM Handbook, Vol. 18 (ASM International, Metals Park, OH, 1992).
[2] M. Minami, M. Suzuki, and M. Nishimura, Proceedings 47th Annual Meeting STLE, Philadelphia, PA, May 4–7, 1992.
[3] R. L. Fusaro, in *Lubrication for Space Applications*, NASA Technical Memorandum 102492 (Lewis Research Center, Cleveland, Ohio, February 1990).
[4] D. H. Buckley, M. Swikert, and R. L. Johnson, ASLE Trans. **6**, 8 (1962).
[5] J. M. Cunningham and C. G. Marirrodriga, in Proceedings Sixth European Mechanisms & Tribology Symposium, Technopak, Zurich, Switzerland, 4–6 October 1995, p. 35.
[6] R. E. Imhof, B. Zhang, and D. J. S. Birch, in Non-Destructive Evaluation, *Progress in Photothermal and Photoacoustic Science and Technology*, Vol. II, edited by A. Mandelis (PTR Prentice Hall, Englewood Cliffs, NJ, 1994), Chap. 7.
[7] A. Mandelis, Rev. Sci. Instrum. **65**, 3309 (1994).
[8] L. M. Dorojkine and A. Mandelis, Opt. Eng. **36**, 473 (1997).
[9] Input offset reduction using the model 7265/7260/7220 synchronous oscillator/demodulator monitor output, Application Note AN 1001, EG&G Signal Recovery, TN 37831-2011, 1999.
[10] A. Mandelis, *Diffusion-Wave Fields: Green Functions and Mathematical Methods* (Springer, New York, in press).
[11] I. S. Gradshteyn and I. M. Ryzhik, *Table of Integrals, Series and Products* (Academic, Orlando, 1980).
[12] J. R. Markham and K. Kinsella, Int. J. Thermophys. **19**, 537 (1998).